Engineering the Search for New Worlds

Cornell MAE Seminar

Dmitry Savransky

October 20, 2020

Portions of this work supported by NASA grants NNX15AJ67G and NNX15AB40G, and NSF grant 1920180

Introducing SIOSlab

CARL SAGAN INSTITUTE

THE PALE BLUE DOT & BEYOND.

The Carl Sagan Institute was founded to find life in the universe

27 faculty (+ researchers and students) from 4 Colleges and 14 departments at Cornell University

FOUNDING DIRECTOR:
Lisa Kaltenegger

DEPUTY DIRECTOR:
Nikole Lewis

SCIENCE BOARD:
Members from Astronomy, MAE, EAS, Biology, Science Communications, and Ann Druyan

So Many Ways to Find a Planet

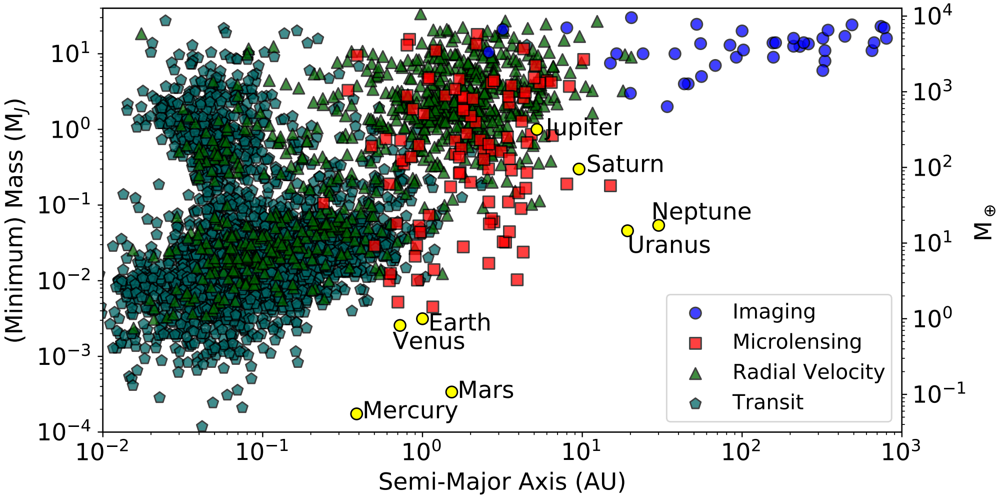

4292 known exoplanets, retrieved 10.13.2020 from the NExSci Exoplanet Catalog

Direct Imaging Pushes Boundaries

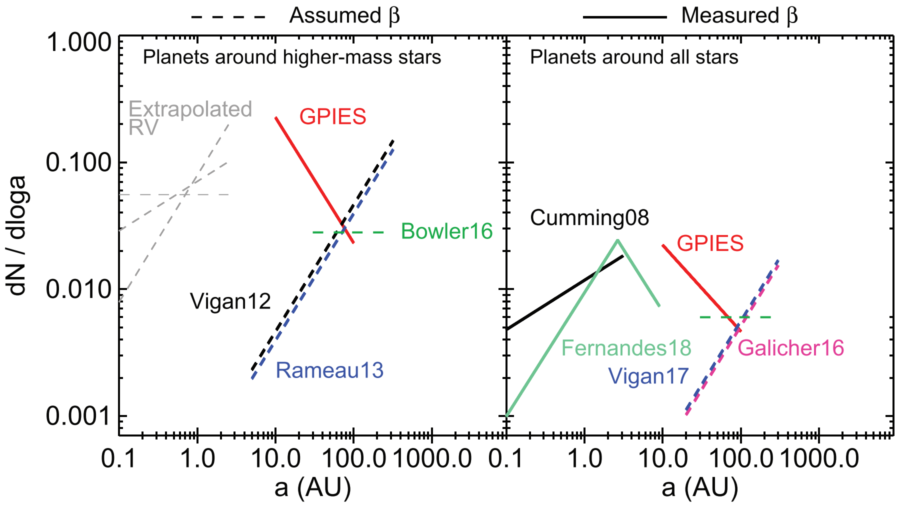

Occurrence rates of 5-13 M_J planets assuming $f_{\bar{a}} \propto a^{\beta}$. Figure from Nielsen et al., “The Gemini Planet Imager Exoplanet Survey: Giant Planet and Brown Dwarf Demographics from 10 to 100 au”, 2019.

We Have Seen (Some) Light

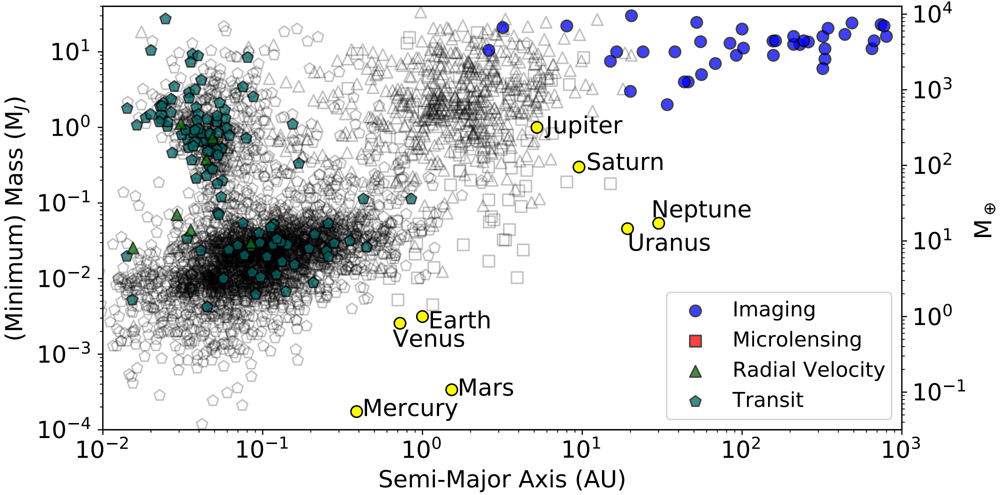

169 planets (51 directly imaged) have any sort of spectra/photometry

Photons are Precious

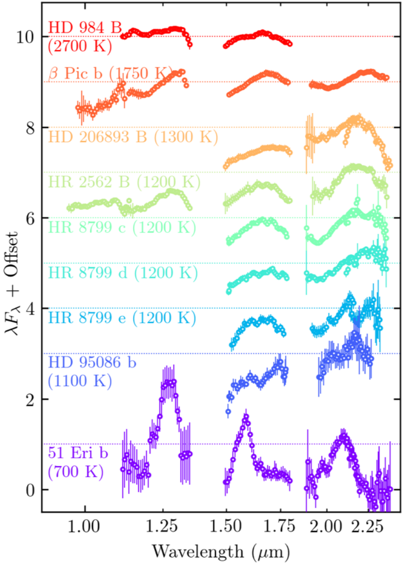

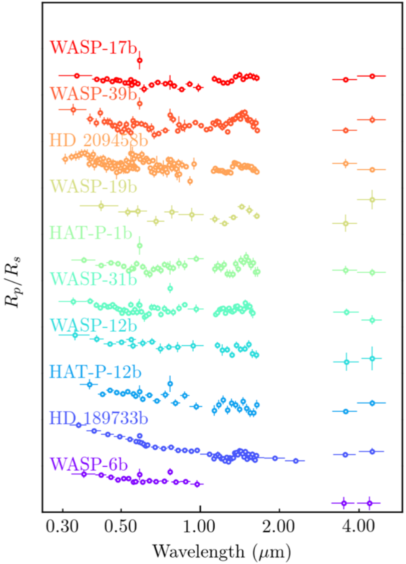

Left: GPIES Spectral Library.
Right: HST/Spitzer transmission spectra, adapted from Sing et al., "A continuum from clear to cloudy hot-Jupiter exoplanets without primordial water depletion", 2016.
Figures by Julien Rameau and Rob De Rosa.

Imaging Constraints

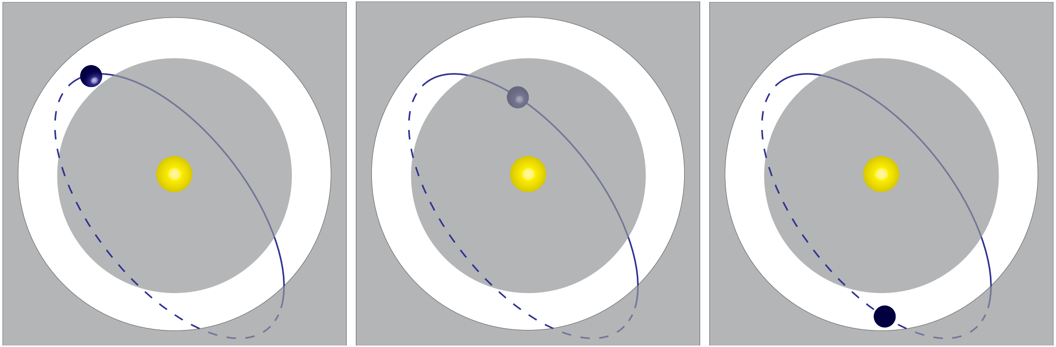

Schematic of projected exosystem. Planet is sufficiently illuminated for detection in reflected light on solid part of orbit, and observable outside the gray region.

All imaging systems have an inner/outer working angle (IWA/OWA) and a limiting planet/star flux ratio (function of angular separation).

Imaging Observables (Geometry)

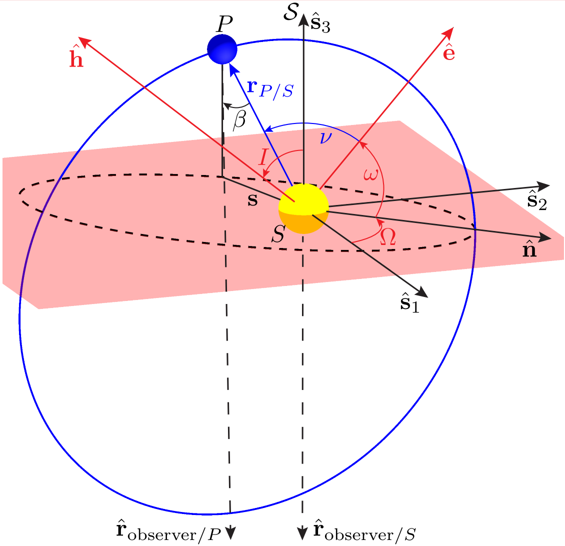

$$\theta = \nu + \omega$$

$$r = \|\mathbf{r}_{P/S}\|$$

$$\begin{aligned} s =& \|\mathbf{r}_{P/S} - (\mathbf{r}_{P/S} \cdot \hat{\mathbf{s}}_3)\hat{\mathbf{s}}_3\| \\ =& \frac{r}{4}\left[4\cos(2I) + 4\cos(2\theta) \right. \\ & - 2\cos(2I - 2\theta) \\ & \left. - 2\cos(2I + 2\theta) + 12\right]^{-\frac{1}{2}} \end{aligned}$$

$$\beta \approx \cos^{-1}\left(\frac{\mathbf{r}_{P/S} \cdot \hat{\mathbf{s}}_3}{r}\right)$$

$$\cos\beta = \sin(I)\sin(\theta)$$

Imaging Observables (Photometry)

Energy per second per unit area per unit solid angle received by an observer =

$$\frac{FR^2}{r^2}\int_{\beta-\pi/2}^{\pi/2}\cos(\beta-\delta)\cos\delta\,\mathrm{d}\delta\int_{-\pi/2}^{\pi/2}\rho(C_\mu, C_\gamma, \xi)\cos^3\alpha\,\mathrm{d}\alpha$$

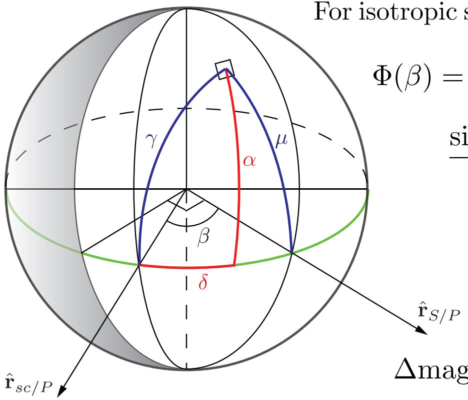

For isotropic scattering, ρ = constant

$$\Phi(\beta) = \frac{E(\beta)}{E(0)} = \frac{\sin(\beta) + (\pi-\beta)\cos(\beta)}{\pi}$$

$$\frac{F_p}{F_S} = p\Phi(\beta)\left(\frac{R}{r}\right)^2$$

$$\Delta\mathrm{mag} = -2.5\log_{10}\left(\frac{F_p}{F_S}\right)$$

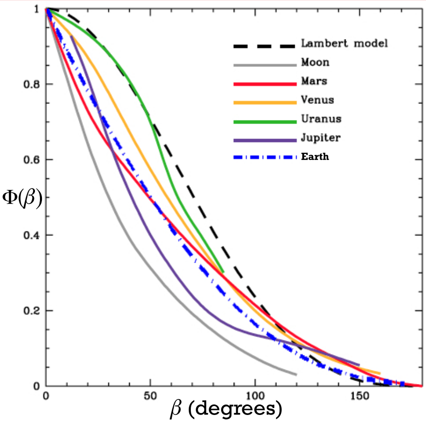

Solar system body and isotropic-scatterer (Lambert) phase functions. Data from Sudarsky et al. (2005) and De Vaucouleurs (1964)

Sampling Geometric Parameters

$\Omega, \omega \sim U([0, 2\pi])$

$I, \beta \sim \cos^{-1}(U([-1, 1]))$

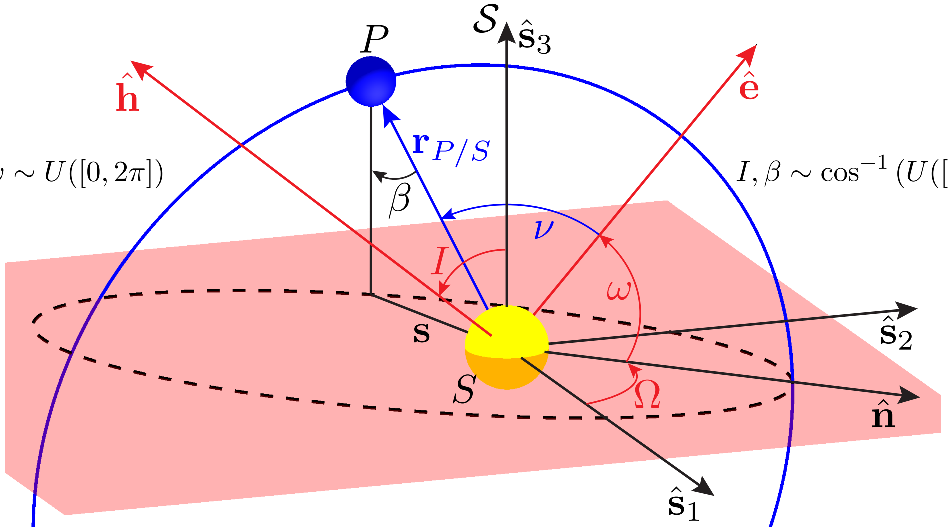

Savransky, Cady, and Kasdin, "Parameter distributions of Keplerian orbits", 2011

Sampling Period and Planet Radius: The SAG13 Universe

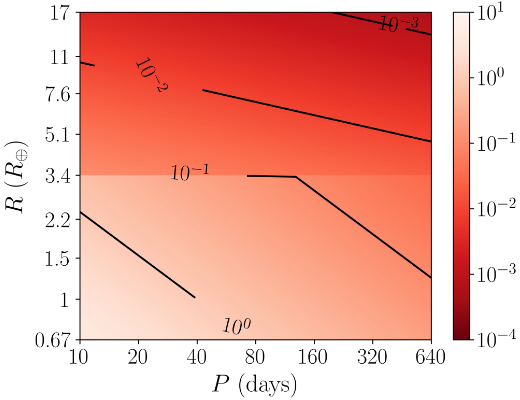

$$\frac{\partial^2 \eta}{\partial \ln R \partial \ln P} = \begin{cases} \Gamma_i R^{\rho_i} P^{\beta_i} & R_{i-1} \leq R < R_i \\ 0 & \text{else} \end{cases}$$

Γ_i	ρ_i	β_i	R_i
0.38	-0.19	0.26	3.4
0.73	-1.18	0.59	∞

Belikov et al. see: https://exoplanets.nasa.gov/exep/exopag/sag/ ▸ More

Sampling Albedo: Model Libraries to the Rescue

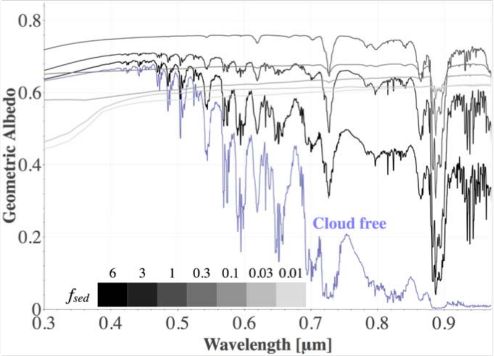

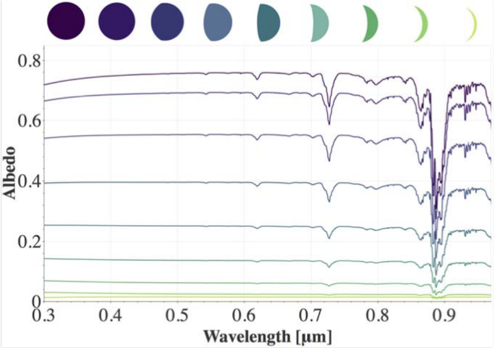

Batalha et al., "Color Classification of Extrasolar Giant Planets: Prospects and Cautions", 2018 ▸ More

The Direct Imaging Joint Probability Distribution

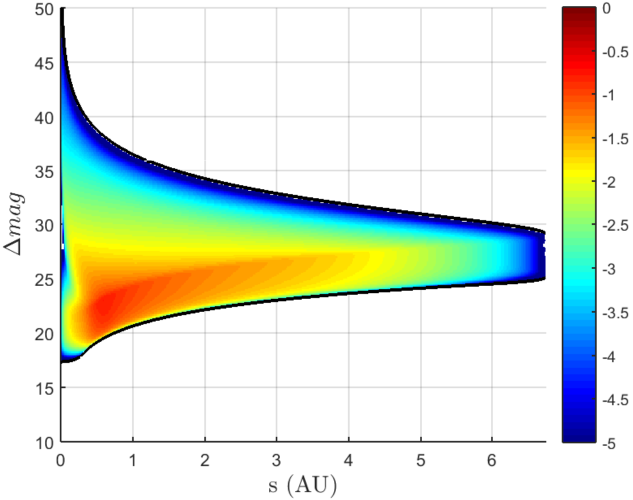

$$f_{\bar{s},\overline{\Delta\text{mag}}}(s,\Delta\text{mag}) = \int_{-\infty}^{\infty}\int_{-\infty}^{\infty} f_{\bar{s},\overline{\Delta\text{mag}},\bar{p},\bar{R}}(s,\Delta\text{mag},p,r)\,\mathrm{d}R\,\mathrm{d}p$$

`github.com/dgarrett622/FuncComp`

Garrett and Savransky, "Analytical Formulation of the Single-visit Completeness Joint Probability Density Function", 2016

Imaging Is Incredibly Difficult!

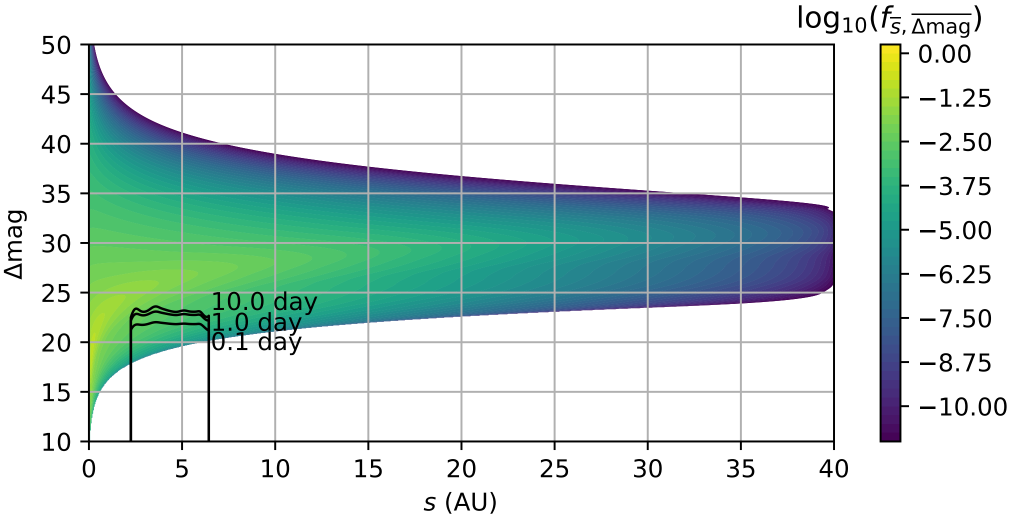

The (Ongoing) Saga of the Nancy Grace Roman Space Telescope

1. 2010: WFIRST identified as top priority by decadal survey
2. 2011 - 2012: DRM 1 concludes with 1.3 m single instrument design
3. Jan 2011: NRO offers NASA two Hubble-class telescope
4. Aug 2011: NASA accepts
5. June 2012: Telescopes declassified, named AFTA
6. Nov 2012: New SDT Formed to study WFIRST-AFTA
7. 2012-2013: Coronagraph added, SDT reformed
8. Jan 2015: SDT produces final report
9. Jan-Feb 2016: WFIRST passes KDP-A; SITs formed
10. Oct 2017: Independent review; CGI reclassified as tech demo
11. March 2018: SRR and MDR passed
12. September 2019: PDR passed
13. March 2020: WFIRST Enters Phase C
14. May 2020: Renamed Nancy Grace Roman Space Telescope
15. September 2020: Primary Mirror Completed

AFTA → WFIRST → Roman

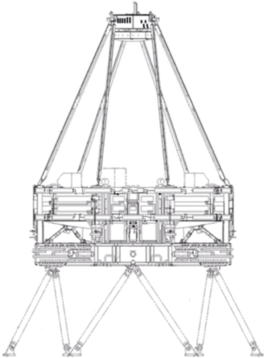

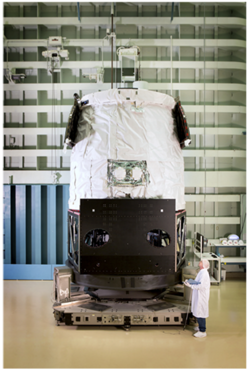
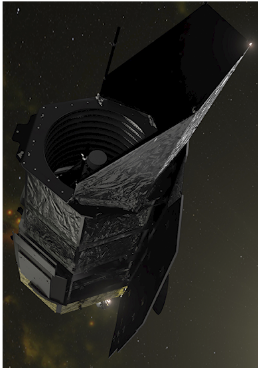

The Roman CGI

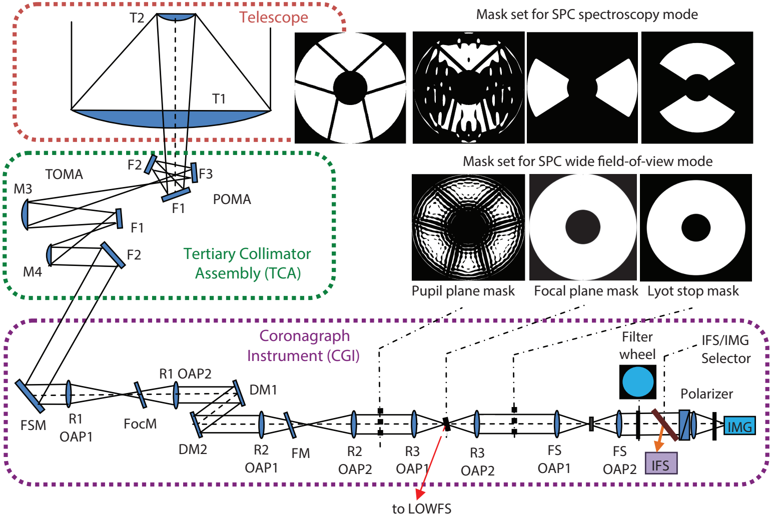

Figure from: Zhou et al., "High accuracy coronagraph flight WFC model for WFIRST-CGI raw contrast sensitivity analysis", 2018

Going for What We Know is There

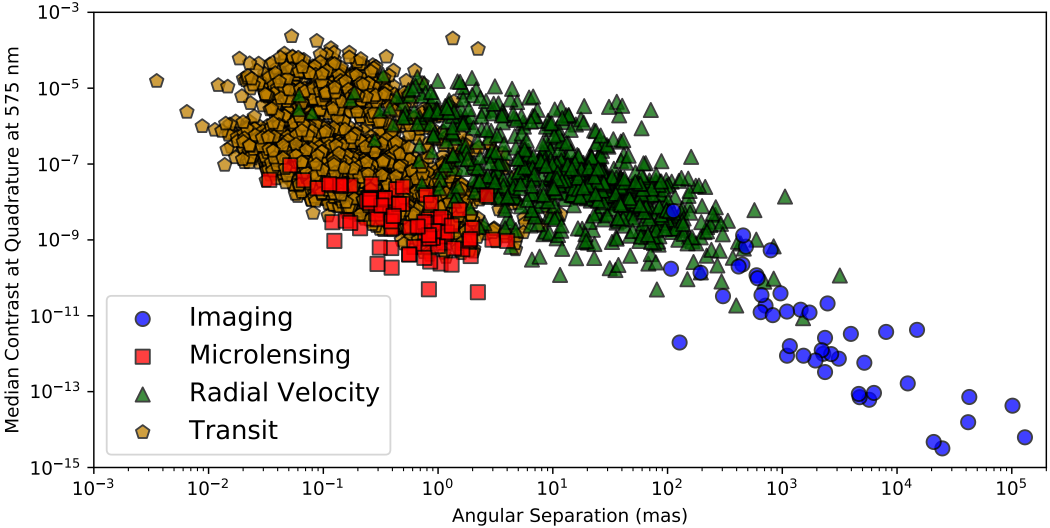

Even If You Know Something is There...

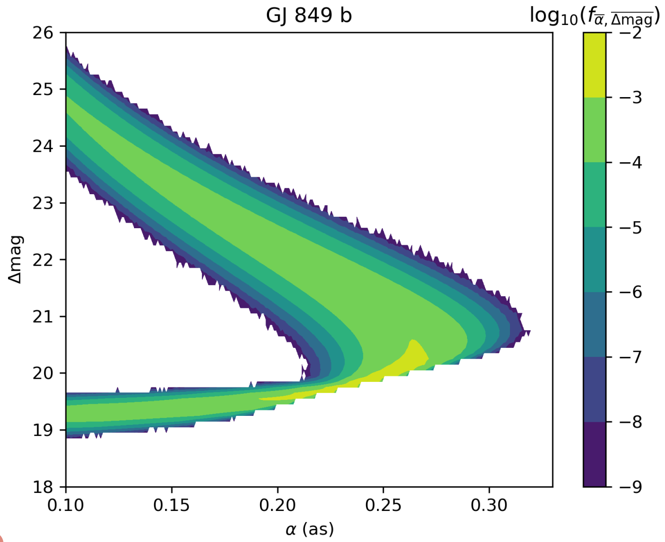

... you still might not see it

▸ More

When Should We Give Up on an Observation?

RV Targets: Orbital & Photometric Uncertainty

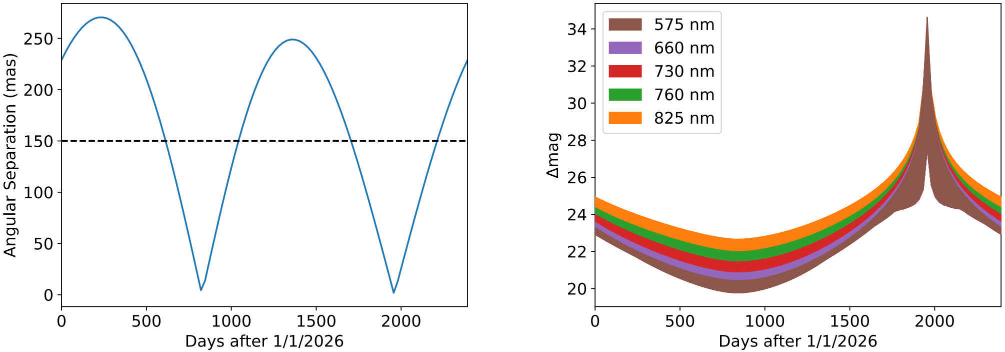

47 UMa c, Assuming 90° Inclination

See: `https://plandb.sioslab.com`

RV Targets: Inclination Uncertainty

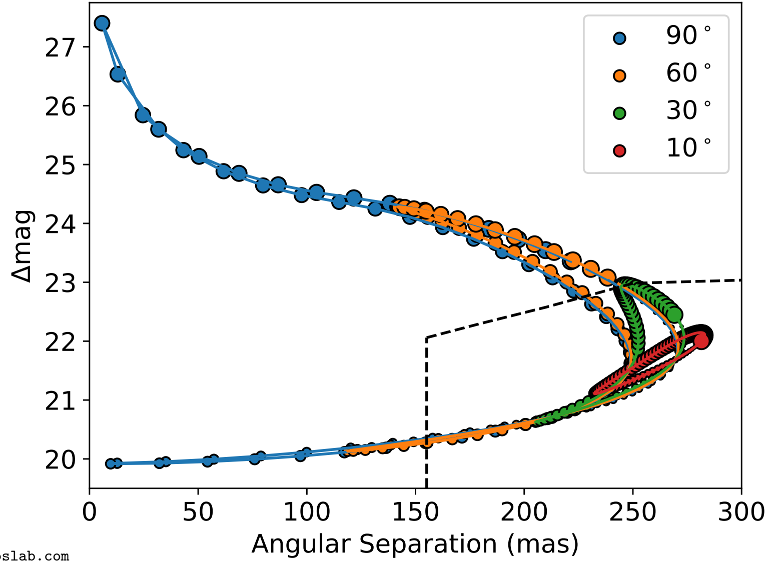

See: `https://plandb.sioslab.com`

There's Definitely a 'Best' Time to Look

Monte Carlo Mission Simulation

→

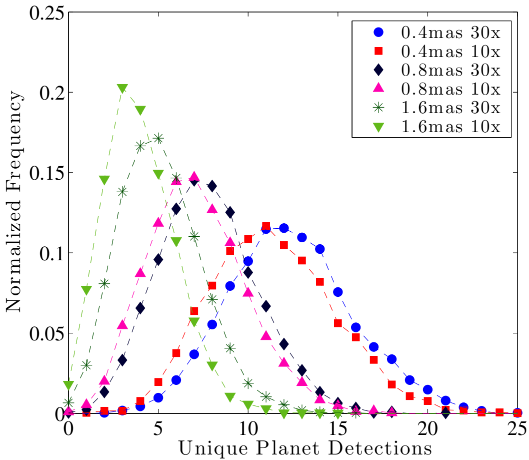

As always: garbage in/garbage out

See: Savransky, Kasdin, and Cady, “Analyzing the designs of planet finding missions”, 2010; Savransky and Garrett, “WFIRST-AFTA coronagraph science yield modeling with EXOSIMS”, 2015

Why Monte Carlo? Dynamic Constraints and Schedulability!

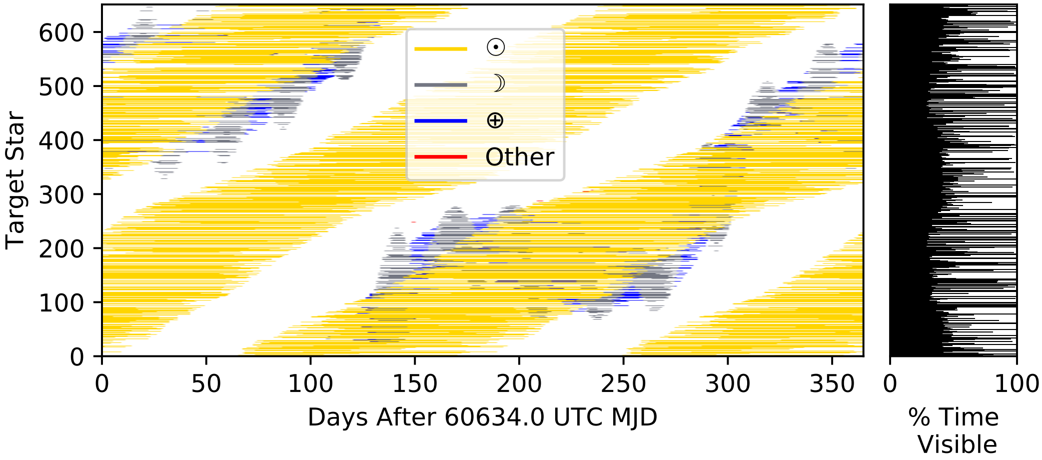

Targets are observable in white regions of the graph. The sun keepout is due to both sun avoidance and solar panel pointing restrictions. More

All the Moving Pieces

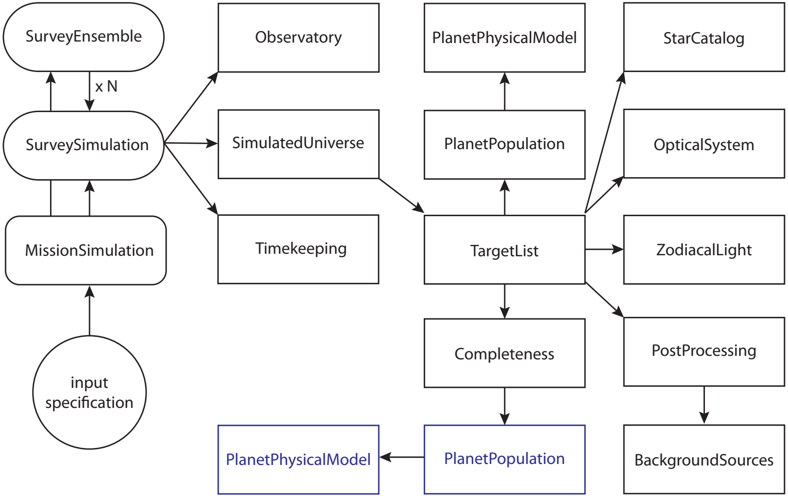

github.com/dsavransky/EXOSIMS

Putting it All Together

See: Savransky, Delacroix, and Garrett, "Multi-mission modeling for space-based exoplanet imagers", 2017 ▸ More

The Gemini Planet Imager

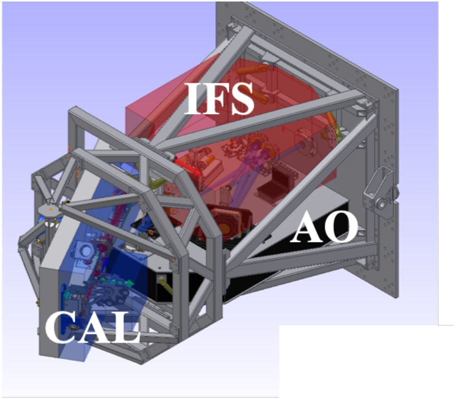

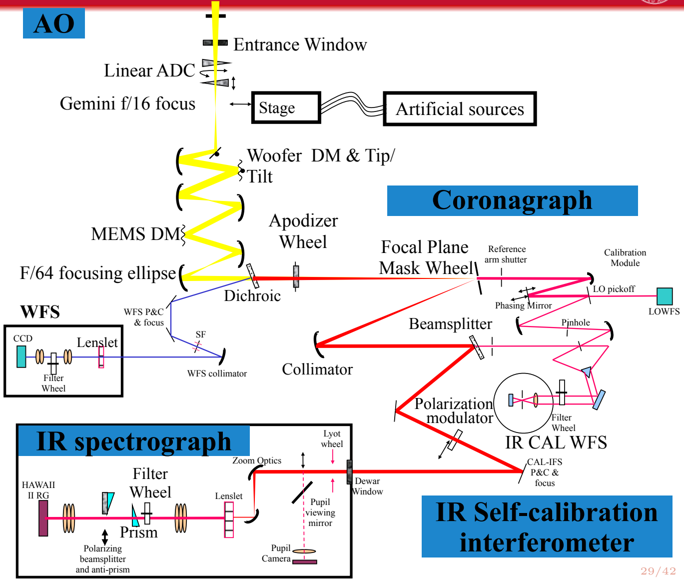

GPI Key Features

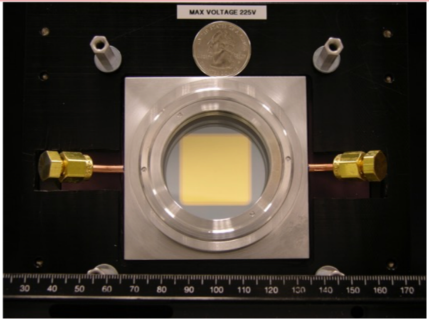

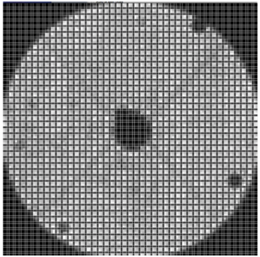

- BMM 4096-actuator MEMS deformable mirror + piezo woofer (5 bad actuators)
- Spatially-filtered Shack-Hartmann WFS with 160x160 pixel Lincoln Labs CCD
- 1 kHz update rate with approximately 1.4 ms delay
- $I < 10$ mag limit
- Superpolished (1nm RMS) optics
- 1—2.5 micron 2.7” × 2.7” FOV IFS

GPI at Gemini South

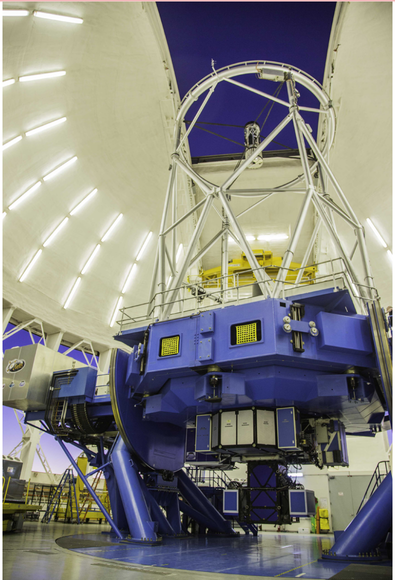

GPIES Campaign Data System

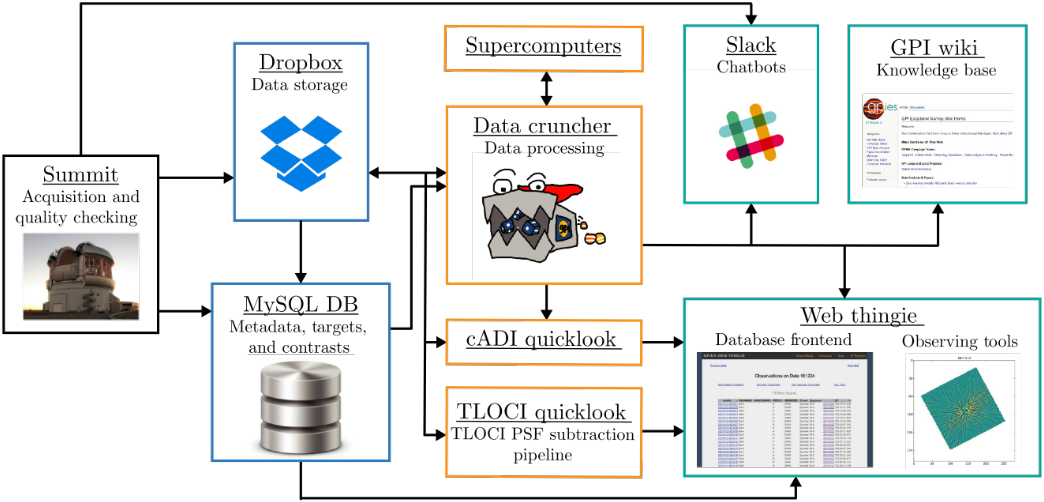

See: Wang et al., "Automated data processing architecture for the Gemini Planet Imager Exoplanet Survey", 2018

Goodbye, Gemini South—Hello, Gemini North

Goodbye, Gemini South—Hello, Gemini North

Exoplanet Survey

GPI 2.0 Science Driver: Hot Start vs Cold Start

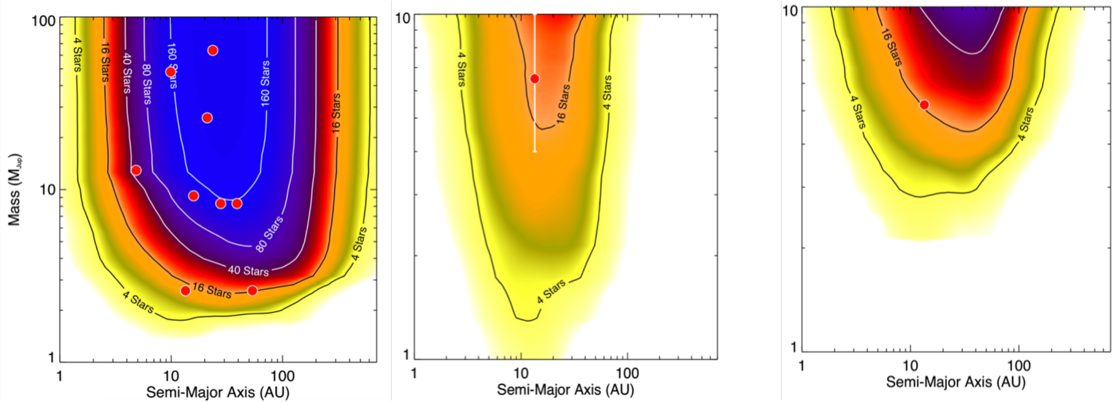

Hot start (BTSET)   Cold start (Fortney 2008)   Cold start (Sonora models)

Nielsen et al., "The Gemini Planet Imager Exoplanet Survey: Giant Planet and Brown Dwarf Demographics from 10 to 100 au", 2019

GPI Now

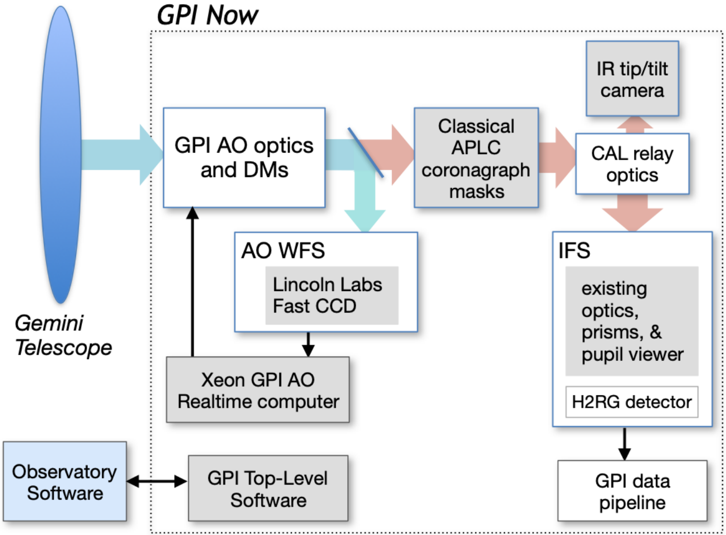

Slide by M. Perrin

GPI 2.0

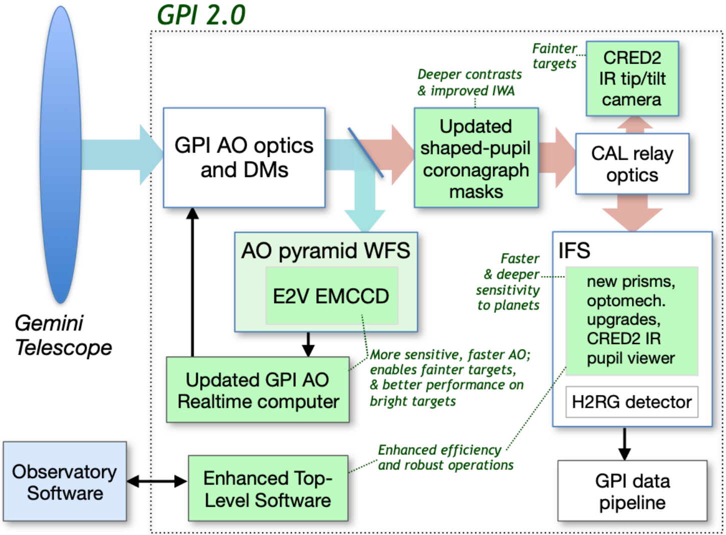

Slide by M. Perrin

Pupil Viewer Upgrades May Enable Better Phase Retrieval

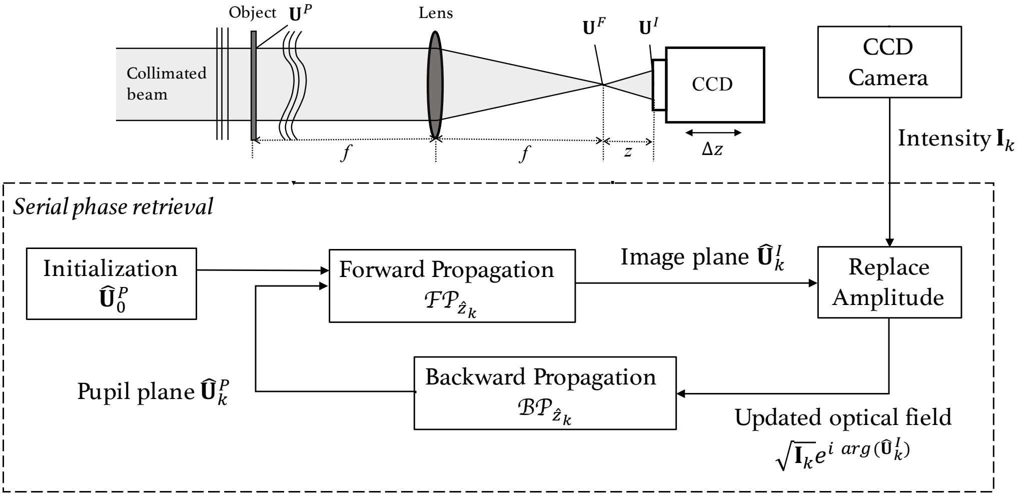

Slide by J. Fang. See: Fang and Savransky, "Wavefront reconstruction with defocus and transverse shift estimation using Kalman filtering", 2018

System Uncertainty Destroys the Result

Input

Reconstruction assuming 1.25% uncertainty in camera position and 0.5 pixel image shifts

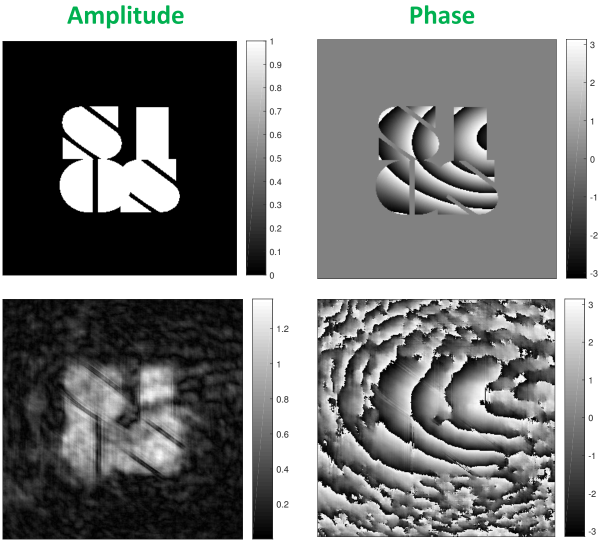

See: Fang and Savransky, "Wavefront reconstruction with defocus and transverse shift estimation using Kalman filtering", 2018

Phase Retrieval with System Misalignment Estimation (Simulation)

Amplitude

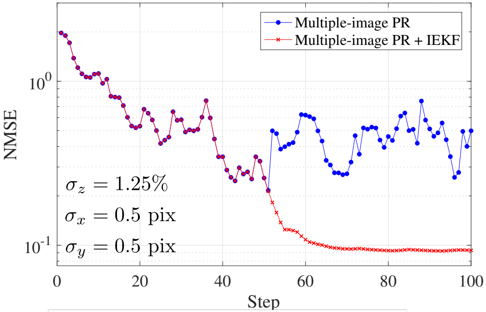

$$\text{NMSE} = \min_{\phi_c} \frac{\sum_{x,y} \left| \hat{\boldsymbol{U}}^P(x,y) \exp(j\phi_c) - \boldsymbol{U}^P(x,y) \right|^2}{\sum_{x,y} \left| \boldsymbol{U}^P(x,y) \right|^2}$$

Retrieval | Retrieval + IEKF

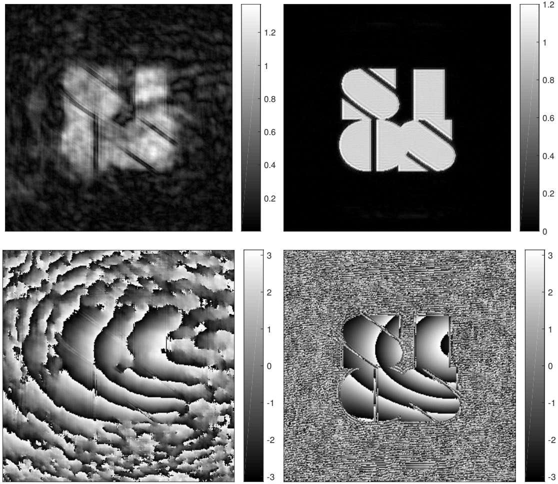

Phase

Laboratory Result

Amplitude

\+

Convex Lens
EFL = 1000 mm
BFL = 995.3 mm

Phase

Retrieval

Retrieval + IEKF

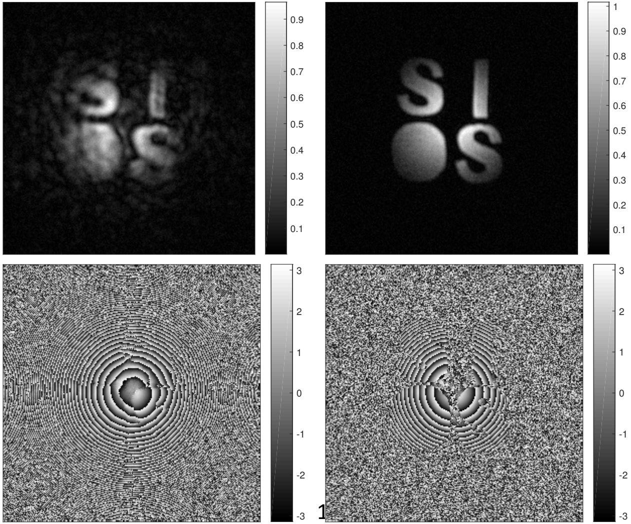

Phase Unwrapping

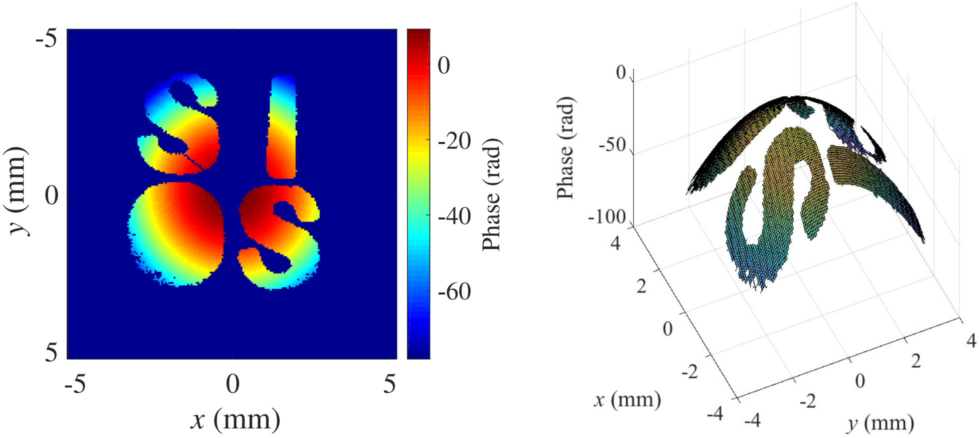

Manufacturer specification: BFL = 995.3 mm (± 1 %)

Estimated BFL: 997.6 mm

See: Fang and Savransky, "Wavefront reconstruction with defocus and transverse shift estimation using Kalman filtering", 2018

GPIES

References I

- Batalha, Natasha E et al. (2018). "Color Classification of Extrasolar Giant Planets: Prospects and Cautions". In: *The Astronomical Journal* 156.4, p. 158.
- Fang, Joyce and Dmitry Savransky (2018). "Wavefront reconstruction with defocus and transverse shift estimation using Kalman filtering". In: *Optics and Lasers in Engineering* 111, pp. 122 –129. ISSN: 0143-8166. DOI: https://doi.org/10.1016/j.optlaseng.2018.07.006. URL: http://www.sciencedirect.com/science/article/pii/S0143816618304329.
- Garrett, Daniel and Dmitry Savransky (2016). "Analytical Formulation of the Single-visit Completeness Joint Probability Density Function". In: *The Astrophysical Journal* 828.1, p. 20. URL: http://stacks.iop.org/0004-637X/828/i=1/a=20.
- Hunyadi, S. L., A. S. Lo, and S. B. Shaklan (2007). "The dark side of TPF: detecting and characterizing extra-solar Earthlike planets with one or two external occulters". In: *Proc SPIE*. Vol. 6693, p. 669303.

References II

- Kraft, Dieter (1994). "Algorithm 733: TOMP–Fortran modules for optimal control calculations". In: *ACM Transactions on Mathematical Software (TOMS)* 20.3, pp. 262–281.
- Nemati, Bijan, John E Krist, and Bertrand Mennesson (2017). "Sensitivity of the WFIRST coronagraph performance to key instrument parameters". In: *Techniques and Instrumentation for Detection of Exoplanets VIII*. Vol. 10400. International Society for Optics and Photonics, p. 1040007.
- Nielsen, Eric L. et al. (2019). "The Gemini Planet Imager Exoplanet Survey: Giant Planet and Brown Dwarf Demographics from 10 to 100 au". In: *The Astrophysical Journal* 158.1, 13, p. 13. DOI: 10.3847/1538-3881/ab16e9. arXiv: 1904.05358 [astro-ph.EP].
- Savransky, D., E. Cady, and N .J. Kasdin (2011). "Parameter distributions of Keplerian orbits". In: *The Astrophysical Journal* 728.1, p. 66.

References III

- Savransky, D., N. J. Kasdin, and E. Cady (2010). "Analyzing the designs of planet finding missions". In: *Publications of the Astronomical Society of the Pacific* 122.890, pp. 401–419.
- Savransky, Dmitry, Christian Delacroix, and Daniel Garrett (Sept. 2017). "Multi-mission modeling for space-based exoplanet imagers". In: *Society of Photo-Optical Instrumentation Engineers (SPIE) Conference Series*. Vol. 10400, 104001L, p. 104001L. DOI: 10.1117/12.2274098.
- Savransky, Dmitry and Daniel Garrett (2015). "WFIRST-AFTA coronagraph science yield modeling with EXOSIMS". In: *Journal of Astronomical Telescopes, Instruments, and Systems* 2.1, p. 011006. DOI: 10.1117/1.JATIS.2.1.011006. URL: http://dx.doi.org/10.1117/1.JATIS.2.1.011006.

References IV

- Sing, David K. et al. (2016). "A continuum from clear to cloudy hot-Jupiter exoplanets without primordial water depletion". In: *Nature* 529.7584, pp. 59–62. DOI: 10.1038/nature16068. arXiv: 1512.04341 [astro-ph.EP].
- Wang, Jason J et al. (2018). "Automated data processing architecture for the Gemini Planet Imager Exoplanet Survey". In: *Journal of Astronomical Telescopes, Instruments, and Systems* 4.1, p. 018002.
- Williams, H Paul (2009). *Logic and integer programming*. Springer.
- Zhou, Hanying et al. (2018). "High accuracy coronagraph flight WFC model for WFIRST-CGI raw contrast sensitivity analysis". In: *Space Telescopes and Instrumentation 2018: Optical, Infrared, and Millimeter Wave*. Vol. 10698. International Society for Optics and Photonics, p. 106982M.

Extrapolating SAG13

- Change to radius—semi-major axis space:

$$\frac{\partial^2 \eta}{\partial R \partial P} = \Gamma_i R^{\rho_i - 1} \left(2\pi \sqrt{\frac{a^3}{\mu}} \right)^{\beta_i - 1} \left(3\pi \sqrt{\frac{a}{\mu}} \right)$$

- Include semi-major axis decay:

$$\frac{\partial^2 \eta}{\partial R \partial P} = \Gamma_i R^{\rho_i - 1} \left(2\pi \sqrt{\frac{a^3}{\mu}} \right)^{\beta_i - 1} \left(3\pi \sqrt{\frac{a}{\mu}} \right) e^{-\left(\frac{a}{a_k}\right)^3}$$

The SAG13 Universe Extrapolated

Return

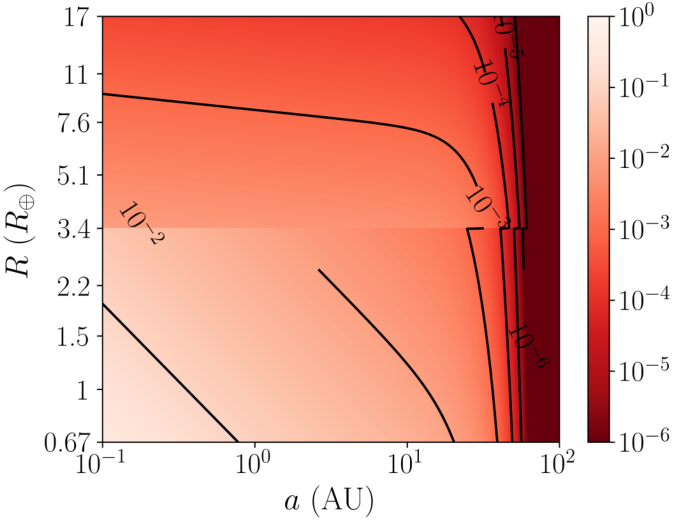

$a_k = 30$ AU

$\eta = 10.7$

Clouds Make a Huge Difference

Return

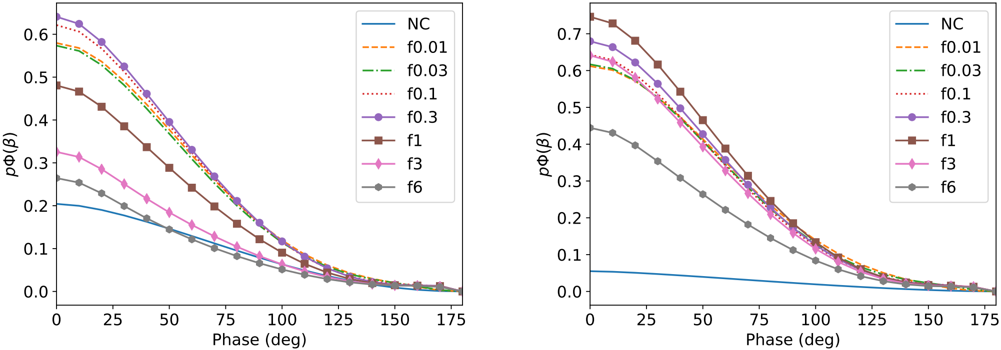

Phase curves for 1 R_J planet at 1 AU / 575 nm *(left)* and 5 AU / 825 nm *(right)*

See: https://plandb.sioslab.com/docs/html/index.html

Discovered Planets Retain Lots of Uncertainty

Return

Roman Keepout Geometry

Return

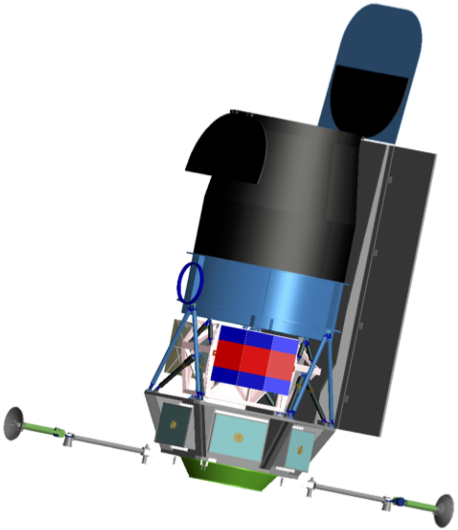

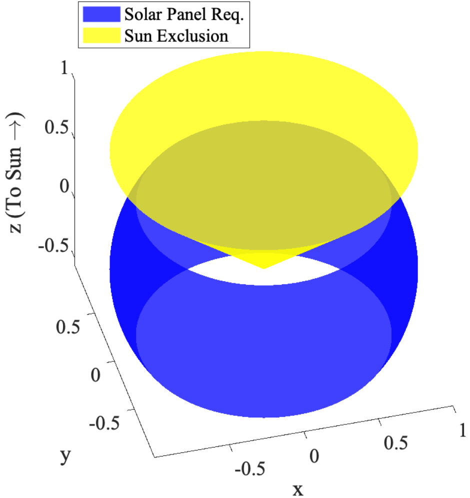

Completeness is the Prize Heuristic

$$c = \int_{\Delta\mathrm{mag}_{\min}(s_{\min})}^{\Delta\mathrm{mag}_u} \int_{s_{\min}}^{s_u(\Delta\mathrm{mag})} f_{\bar{s},\overline{\Delta\mathrm{mag}}}(s, \Delta\mathrm{mag})\, \mathrm{d}s\, \mathrm{d}\Delta\mathrm{mag}.$$

(See Garrett and Savransky, “Analytical Formulation of the Single-visit Completeness Joint Probability Density Function”, 2016)

$$\Delta\mathrm{mag}(t) = -m - 2.5\log_{10}\left(\frac{\mathrm{SNR}}{\mathcal{F}_0 T}\sqrt{\frac{C_b}{t} + C_{sp}^2}\right)$$

(See Nemati, Krist, and Mennesson, “Sensitivity of the WFIRST coronagraph performance to key instrument parameters”, 2017)

$$\frac{\mathrm{d}\Delta\mathrm{mag}}{\mathrm{d}t} = \frac{5C_b}{4\ln(10)}\frac{1}{C_b t + (C_{sp}t)^2}$$

$$\left.\frac{\mathrm{d}c}{\mathrm{d}t}\right|_{t_{\mathrm{int}}} = \left[\int_{s_{\min}}^{s_u(\Delta\mathrm{mag}(t_{\mathrm{int}}))} f_{\bar{s},\overline{\Delta\mathrm{mag}}}(s, \Delta\mathrm{mag}(t_{\mathrm{int}}))\, \mathrm{d}s\right] \left.\frac{\mathrm{d}\Delta\mathrm{mag}}{\mathrm{d}t}\right|_{t_{\mathrm{int}}}$$

Target Selection

You are very likely to have more available targets than mission time

so make the best use of your available time

$$\arg\min_{\{t_i\}} \left(-\sum_{i}^{n} c_i(t_i) \right)$$

subject to:

$$t_{\max} - \sum_{i}^{n} t_i - \left(\sum_{i}^{n} t_i^{\text{over}}(t_i > 0) \right) \geq 0$$

such that:

$$0 \leq t_i \leq t_{\max} \qquad \forall i \, .$$

See: Hunyadi, Lo, and Shaklan, "The dark side of TPF: detecting and characterizing extra-solar Earthlike planets with one or two external occulters", 2007

Overhead is a Problem

This is an unfriendly constraint:

$$t_{\max} - \sum_{i}^{n} t_i - \left(\sum_{i}^{n} t_i^{\text{over}} (t_i > 0) \right) \geq 0$$

Consider instead:

$$\left.\begin{aligned} &\arg\min_{T} \left(- \sum_{i \in T} c_i \right) \\ &\text{subject to:} \\ &\sum_{i \in T} (t_i + t_i^{\text{over}}) \leq t_{\max} \end{aligned}\right\}$$

$$\arg\min_{\mathbf{x}} \left(-\mathbf{c}^T \mathbf{x} \right) \qquad \mathbf{c}, \mathbf{t} \in \mathbb{R}^N$$

$$(\mathbf{t} + \mathbf{t}^{\text{over}})^T \mathbf{x} < t_{\max}$$

$$\mathbf{x} \in \mathbb{Z}^N$$

$$\mathbf{0} \leq \mathbf{x} \leq \mathbf{1}$$

$$T = \{ i : x_i = 1, \forall x_i \in \mathbf{x} \}$$

Initialisms Galore

- The original problem is a nonlinear optimization:
  - We solve it using Sequential Least-Squares Quadratic Programming (SLSQP; Kraft 1994)
  - This is hard and computationally expensive if you don't start near a local minimum
- The auxiliary fixed integration time problem is a Binary Integer Linear Programming Problem (BILPP; Williams 2009)
  - Actually NP-complete, but computationally cheap for reasonably sized target lists using branch and cut
  - 'Reasonable' $\approx$ 1000 targets

Continuous Completeness Maximization

Return

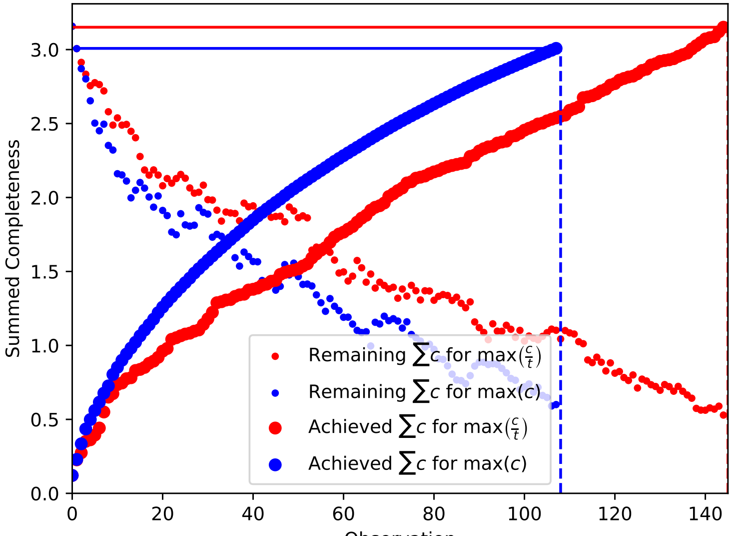

Shack-Hartmann to Pyramid

Return

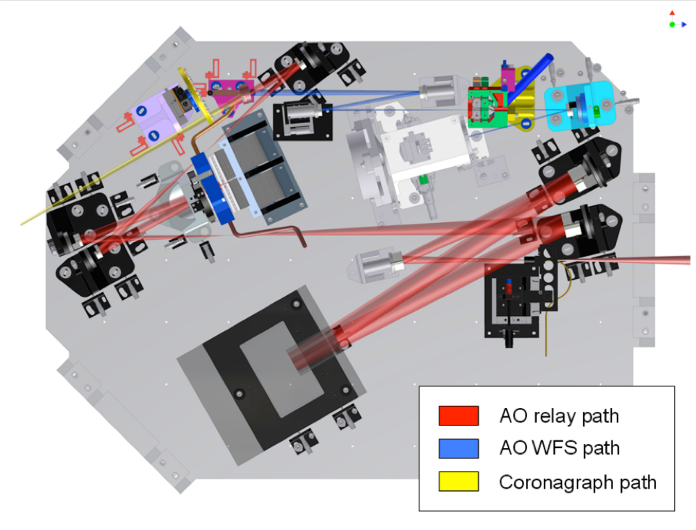

Shack-Hartmann to Pyramid

Return

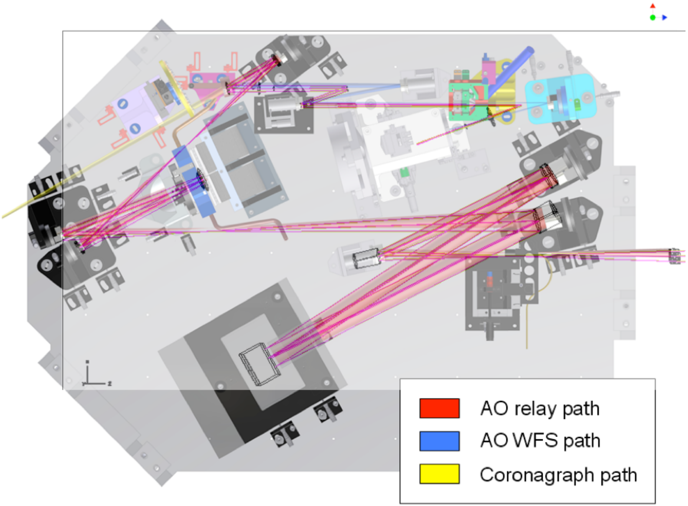

Phase Retrieval with System Misalignment Estimation

Return

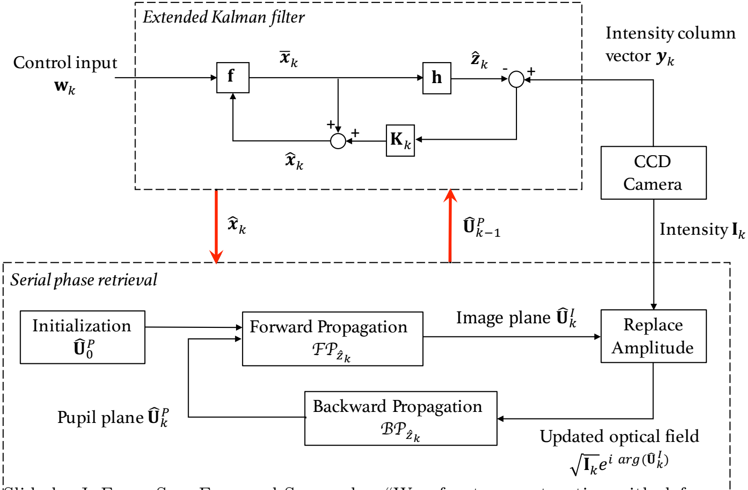

$$x_k = f(x_{k-1}, w_k) + v_k = \begin{bmatrix} z_{k-1} \\ s^x_{k-1} \\ s^y_{k-1} \end{bmatrix} + \begin{bmatrix} \Delta z_k \\ 0 \\ 0 \end{bmatrix} + q_k$$

$$y_k = h(\hat{U}^P_{k-1}, x_k) + r_k = \text{diag}((\hat{u}^I_k)^*)\hat{u}^I_k + r_k$$

Slide by J. Fang. See: Fang and Savransky, "Wavefront reconstruction with defocus and transverse shift estimation using Kalman filtering", 2018